Absorption Spectra Related to Heterogeneous Electron Transfer Reactions: The Perylene TiO₂ System

Luxia Wang,[†] Ralph Ernstorfer,[‡] Frank Willig,[‡] and Volkhard May*,[†]

Institut für Physik, Humboldt−Universität zu Berlin, Newtonstraße 15, D-12489 Berlin, Germany, and Hahn−Meitner−Institut Berlin, Dynamics of Interfacial Reactions−SE 4, Glienicker Str. 100, D-14109 Berlin, Germany

Linear absorption spectra of dye−semiconductor systems (perylene attached to nanostructured TiO₂) are studied theoretically and experimentally. The systems show ultrafast photoinduced heterogeneous electron transfer (HET). By applying a time-dependent formulation of the absorbance, the theoretical analysis of the measured data is carried out. The respective electron-vibrational wave packet propagation fully accounts for the electronic coupling to the conduction band continuum of TiO₂ and is based on a single-reaction-coordinate model (corresponding to a perylene in-plane C−C stretching vibration with a quantum energy of 1370 cm^{-1}). By the insertion of different bridge-anchor groups, the electronic coupling responsible for HET is varied. The dye absorbance in a solvent and the trends in the line broadening of the vibrational progression due to the coupling to the conduction band continuum are reproduced for all investigated types of bridge-anchor groups. HET rates deduced from the calculations on the absorbance displaying line broadenings follow the qualitative trend obtained from transient absorption spectra.

I. Introduction

The study of heterogeneous electron transfer (HET) in nanohybrid systems represents an emerging topic of physical chemistry and materials science.[1] Investigations on photoinduced HET between molecules and solids are aiming at potentially interesting practical device applications.[2−7] In addition, the exploration of the unique properties of such heterogeneous interfaces as connections between molecules and macroscopic systems is an interesting topic in its own rights. For example, HET may be used as a model for studying the strength of electronic coupling through specific molecular bridge units in the absence of complications arising from Franck−Condon factors.[8] Such information on the electronic coupling strength is much more difficult to identify unambiguously in other experimental systems where the so-called wide band limit cannot be realized.[2,9−13]

Hitherto, experimental work addressing ultrafast HET has focused on gathering time resolved data. This might be possible either from femtosecond transient absorption signals obtained at colloidal systems, where in fortunate cases the reactant as well as the product states can be probed with the respective absorption signals,[14−16] or from femtosecond two-photon photoemission signals.[17,18] Here, the same electron transfer process can be studied on the surface of single crystals. However, the interpretation of the potentially more complete experimental data, revealing the time-dependent energy distribution, requires additional information about the electronic states of the system.[19]

Of course, one may also use frequency-domain techniques to get access to the time scale of the interfacial electron transfer process. For example, absorption band broadening can be related to the characteristic time of HET. If the charge injection process into the band continuum is fast, every vibrational state of the excited dye has a short lifetime; that is, it becomes lifetime broadened. Although this effect is well understood in principle, we are not aware of a systematic study of this broadening, in particular by changing the coupling strength of the dye to the conduction band continuum.

It is the aim of the present paper to explore the relationship between absorption spectra and the rate of HET for a series of experimental systems with different electronic coupling strengths. Therefore, the same aromatic chromophore (perylene) functions as the electron donor, with its excited electronic state sufficiently high above the conduction band edge of a wide band gap semiconductor (TiO₂ anatase). The latter serves as the electron acceptor. The strength of electronic coupling is changed when a different bridge-anchor group is inserted between electron donor and acceptor (see Figure 1). To get access to the different coupling strengths, related absorption spectra are analyzed. We concentrate on their line width and apply a quantum mechanical model that can reveal a systematic trend in the data while making use of a minimum set of input parameters.

In general, several vibrational modes will contribute to the absorption spectrum of any aromatic chromophore and this holds true also in the case of perylene.[21,20] The room temperature spectra, however, can be simulated rather well by a single-mode description. Including more vibrational modes which couple to the electronic transition is possible and may improve the fit of the measured data. However, at the same time, this would require the introduction of many more parameters into the fit, which makes the whole procedure rather ambiguous. An alternative, of course, would be the consideration of all modes but based on electronic structure calculations as it has been done for other polyatomic systems of similar complexity (see, for example, ref 22). Since our aim here is testing the qualitative trend in the line width of the different absorption spectra and comparing it with the trend seen in the measured rate constant,

[†] Humboldt−Universität zu Berlin.
[‡] Hahn−Meitner−Institut Berlin.
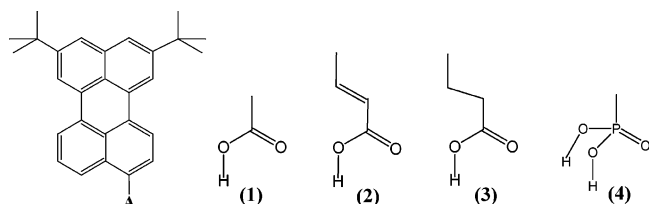
Figure 1. Core chromophore DTB−Pe−A (di-tertiary-butyl perylene, left-most structure) with bridge-anchor groups (right structures) in position A studied in this paper: **1**, −COOH (carboxylic acid); **2**, −(CH)$_2$−COOH (acrylic acid); **3**, −(CH$_2$)$_2$−COOH (proprionic acid); **4**, −P(O)(OH)$_2$ (phosphonic acid).

it appears sufficient and advantageous to keep the number of fit parameters as small as possible.

In the following section, we give some remarks on the experimental work and introduce the model on which the simulations are based. Section III shortly reviews the method used to compute the absorbance (some background information and computational details may be found in the appendix). The comparison between measured and computed spectra is given in section IV. There, the line widths obtained from the simulations are related to HET rates, which are found to qualitatively reproduce the trend seen in the experimental data. The paper ends with some concluding remarks.

II. The TiO$_2$ Chromophore System: Structure and Theoretical Model

Linear absorption spectra were measured at room temperature with UV−vis−NIR spectrometers (Bruins Instruments Omega 10 and 20). The interface was prepared by immersing a transparent nanostructured layer (2 μm thick) composed of anatase colloids (15 nm mean diameter) into a typically 10^{-4} M solution of the respective dye in toluene at room temperature. An absorbance in the range of 0.5 OD was obtained with a contact time of about 10 min for the dyes with the −COOH anchor group and of about 20 min for the dye with the −P(O)-(OH)$_2$ anchor group. Details concerning sample preparation, measurements, and data evaluation have been described already elsewhere.[8] The strength of the electronic coupling between the excited donor state of the perylene chromophore and the empty electronic acceptor states of the TiO$_2$ colloid was varied by inserting the four different bridge-anchor groups shown in Figure 1. To get access to some characteristics of HET, for example, the charge injection time, the absorption spectra of dissolved perylene have been compared with those taken for perylene adsorbed at TiO$_2$.

To deduce different parameters from the measured linear absorption related to HET reactions, we use a model already applied in our former studies.[9−12] It is based on a certain diabatization of the electronic level scheme by introducing the ground state and the first excited state of the dye, φ_g and φ_e, respectively, as well as the large number of states, φ_k, which belong to the conduction band of the semiconductor. The use of a **k** vector is representative of the many conducting states in the TiO$_2$ nanostructure. Probably one may distinguish between more bulklike and more surfacelike states. We will concentrate here, however, on a common class of states with the density of states (DOS) defined below. The energy levels related to the states introduced so far are denoted as E_g, E_e, and E_k. The latter is written as $E_{con} + \hbar\omega_k$, with the lower band edge E_{con} and $\hbar\omega_k$ running over the conduction band with width ΔE_{con} (see Figure 2).
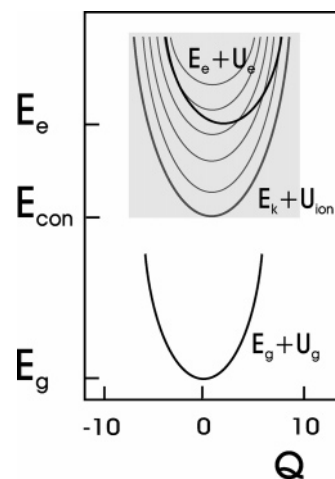
Figure 2. Scheme of PES according to the model Hamiltonian used, eq 2. The positioning of the PES corresponds to the DTB−Pe−COOH−TiO$_2$ system (cf. Figures 1 and 3, note the definition of the reaction coordinate as explained in section 4.1; to avoid confusion, the inclusion of the vibrational zero-point energy into the definition of PES has been neglected).

Charge injection from φ_e into the manifold of states, φ_k, is realized by the transfer coupling, V_{ke}. Of course, this is not a universal quantity but has to account (at least in a semi-phenomenological way) for specific electronic coupling of the chromophore perylene through the bridge-anchor group to the TiO$_2$ nanoparticle surface. For the following, it is customary to change from the **k** dependence of the band energy and the transfer coupling to a continuous frequency dependence by introducing the DOS

$$\mathcal{N}(\Omega) = \sum_{\mathbf{k}} \delta(\Omega - \omega_{\mathbf{k}}) \tag{1}$$

and by replacing V_{ke} by $V_e(\Omega)$.

Any electronic level introduced so far will be complemented by vibrational Hamiltonians, that is, by H_g and H_e for the electronic ground state and the first excited state of the dye, respectively, and by H_{ion} for the ionized dye if charge injection into the conduction band took place. These Hamiltonians include the vibrational kinetic energy operator and the respective potential energy surface (PES) U_g, U_e, and U_{ion}, all drawn in Figure 2. Although we have finally in mind a description using a single vibrational (reaction) coordinate, at the moment, there is no need to specify the vibrational Hamiltonians further. However, to remain sufficiently simple, we make the assumption that the V_{ke} values do not depend on vibrational coordinates.

All contributions discussed here result in the following Hamiltonian of the molecule−semiconductor system (a = g, e, **k**; remember the use of H_{ion} for a = **k**)

$$H_{mol-sem} = \sum_{a=g,e,\mathbf{k}} (E_a + H_a)|\varphi_a\rangle\langle\varphi_a| + \sum_{\mathbf{k}}(V_{ke}|\varphi_{\mathbf{k}}\rangle\langle\varphi_e| +$$
$$\text{h.c.)} \tag{2}$$

For convenience, the electronic energies include the respective vibrational zero-point energies, so the spectrum of the vibrational Hamiltonians starts at zero energy. To proceed further, we introduce the eigenvalues of the diagonal part of $H_{mol-sem}$. If a = g, e, then we write (M stands for the vibrational quantum numbers)

$$E_a + \hbar\omega_{aM} \equiv \hbar(\omega_a + \omega_{aM}) \tag{3}$$

Absorption Spectra Related to HET Reactions

J. Phys. Chem. B, Vol. 109, No. 19, 2005 **9591**

If $a = \mathbf{k}$, we change to the respective frequency dependency and obtain

$$E_{con} + \hbar\omega_\mathbf{k} + \hbar\omega_{ionM} \equiv \hbar(\omega_{con} + \Omega + \omega_{ionM}) \qquad (4)$$

Furthermore, the model assumes that the optical excitation takes place exclusively between the ground state and the excited state of the dye molecule. The related dipole operator takes the following form:

$$\hat{\mu} = \mathbf{d}_{eg}|\varphi_e\rangle\langle\varphi_g| + \text{h.c.} \qquad (5)$$

The transition-dipole matrix element is denoted by $\mathbf{d}_{eg}$ and is taken to be 2.3 D for all perylene bridge-anchor group systems.[20] An excitation into a charge transfer state with the electron directly promoted into the semiconductor conduction band is possible, too, and has been observed for adsorbates forming a chelate-type bond on the surface of TiO_2, for example, the chromophore catechol.[23,24] The electronic coupling strength via acidic groups, however, appears to be weaker. However, it will be demonstrated in the following that the model introduced so far and restricted to a single vibrational coordinate is sufficient to explain the main features of the measured data.

III. The Absorption Coefficient

It represents a standard task to compute linear absorption spectra of molecular systems. Such studies are based on the following formula (cf., e.g., ref 25)

$$\alpha(\omega) = \frac{4\pi\omega n_{mol}}{\hbar c} Re \int_0^\infty dt\, e^{i\omega t} \times \langle\text{tr}\{\hat{W}_{eq}[\hat{\mu}(t), \hat{\mu}]_-\}\rangle_{disorder} \qquad (6)$$

relating the linear frequency resolved absorption to the partial Fourier transformed dipole−dipole correlation function. In the present case, n_{mol} denotes the volume density of the absorbing dye, and the statistical operator, $\hat{W}_{eq}$, describes the thermal equilibrium state of the dye−TiO_2 system before photoabsorption. Moreover, the time dependence of the dipole operator, $\hat{\mu}(t)$, has to be generated by the Hamiltonian $H_{mol-sem}$, eq 2. The system under consideration includes structural and energetic disorder and requires a respective disorder (configuration) averaging symbolized by $\langle ... \rangle_{disorder}$. Since little is known on the details of disorder, the averaging $\langle ... \rangle_{disorder}$ only accounts for random orientation of the dyes (leading to the well-known prefactor $^1/_3$). Other effects are included by an effective level broadening and an effective coupling strength to the band continuum.

Non-Condon effects are of less importance for our further treatment. Therefore, we may introduce the combined DOS, $\mathscr{D}_{abs}$, which enters the absorption via the following relation

$$\alpha(\omega) = \frac{4\pi^2\omega n_{mol}}{3c}|\mathbf{d}_{eg}|^2 \mathscr{D}_{abs}(\omega) \qquad (7)$$

The respective expression of the combined DOS is given in Appendix A. To compute the different measured spectra, we use a method based on time-domain simulations; that is, $\mathscr{D}_{abs}$ is expressed by a wave function correlator (see, for example, ref 25). This requires a direct solution of the time-dependent Schrödinger equation governing the electron-vibrational dynamics of HET (cf. the appendix). However, such an approach masks the absorption line broadening due to the coupling to the band continuum. Changing to an alternative way of calculating $\mathscr{D}_{abs}$,[26]

the broadening effect can be accounted for by (cf. the notation in eq 4)

$$\Sigma(\omega) = \frac{1}{\hbar^2}\sum_\mathbf{k}\frac{|V_{e\mathbf{k}}|^2}{\omega - \omega_{\mathbf{k},e} + i\epsilon}$$

$$\equiv \frac{1}{\hbar^2}\int d\Omega \frac{\mathscr{N}(\Omega)|V_e(\Omega)|^2}{\omega - [\Omega + \omega_{con} - \omega_e] + i\epsilon} \qquad (8)$$

This quantity represents the self-energy (of the vibrational levels in the excited electronic state) due to the coupling to the band continuum. The presence of $\Sigma(\omega)$ in the combined DOS, $\mathscr{D}_{abs}$, indicates the generalization of the Fano-effect to the case of many vibrational transitions coupled to a continuum (for more details cf. ref 26).

Now, let us turn back to the computation of the different measured spectra by using time-domain simulations. In Appendix A, the following formula for the combined DOS has been derived:

$$\mathscr{D}_{abs}(\omega) = \frac{1}{\pi\hbar}Re \int_0^\infty dt\, e^{i(\omega - \omega_{eg})t} \times \sum_M e^{i\omega_e t}\langle\chi_{g0}|\chi_{eM}\rangle C_{eM}(t) \qquad (9)$$

It is based on the solution of the time-dependent Schrödinger equation for the perylene TiO_2 system with an initial condition where the vibrational ground state, χ_{g0}, of the electronic ground state has been put into the excited electronic PES. The $C_{eM}(t)$ values are the related time-dependent expansion coefficients. They follow from an expansion of the complete state vector with respect to the electron-vibrational states, $|\chi_{aM}\rangle|\varphi_a\rangle$, but with a restricted to e and $\mathbf{k}$ (there is no ground-state excited-state coupling in the Hamiltonian, eq 2). If the $C_{eM}(t)$ values are computed for a certain time interval limited by dephasing, they can be inserted into eq 9. To include dephasing, an overall dephasing rate, γ, is introduced by replacing ω by $\omega + i\gamma$. The concrete value of γ is determined within the spectra fit.

The computation of the expansion coefficients, $C_{aM}(t)$, for the case of a single vibrational coordinate has been discussed at length in our foregoing papers.[10−12] It makes use of an expansion of $\mathbf{k}$-dependent, that is, frequency-dependent, quantities with respect to an orthogonal set of functions, $u_r(\Omega)$. For example, one replaces $C_{\mathbf{k}M}(t)$ by $C_M(\Omega;t)$ and the expansion leads to $\sum_r u_r(\Omega)\, C_M^{(r)}(t)$. An appropriate truncation of this summation results in a finite set of coefficients. The frequency dependence of the transfer coupling, $V_e(\Omega)$, and that of the DOS, eq 1, are considered in the same way. All results presented in the following have been obtained in applying this expansion here again. As in refs 10−12, we use Legendre polynomials for $u_r(\Omega)$ up to an order of $r = 200$.

IV. Simulation of Measured Spectra

Our following considerations will be focused on the calculation of absorption spectra of perylene attached to a TiO_2 surface (in high vacuum). Since also solvent spectra of all types of perylene bridge-anchor group systems are available, we may determine internal molecular properties (vibrational frequencies, Stokes shift of the S_0−S_1 transition, etc.) first and independently. Then, in a second step, the model is enlarged by accounting for the conduction band continuum and by fixing the newly appearing parameters. Moreover, our studies will be confronted with old photoionization spectra.[27]
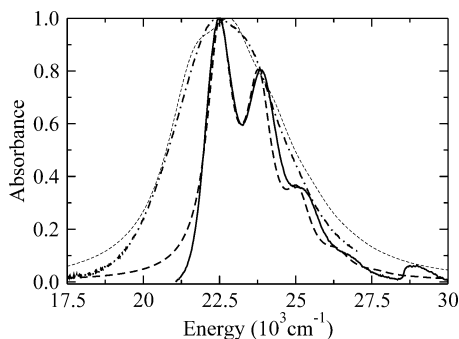
Figure 3. Rescaled linear absorption spectrum of the DTB−Pe−COOH system: solid line, experimental data for the system in the solvent; dashed−dotted line, experimental data for the system adsorbed at a TiO$_2$ surface; thick dashed line, calculated data for the system in the solvent; thin dashed line, calculated data for the system adsorbed at a TiO$_2$ surface (for the parameters used, see Table 1).
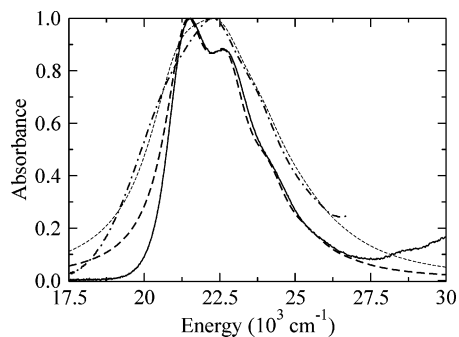
Figure 4. Rescaled linear absorption spectrum of the DTB−Pe−(CH)$_2$−COOH system: solid line, experimental data for the system in the solvent; dashed−dotted line, experimental data for the system adsorbed at a TiO$_2$ surface; thick dashed line, calculated data for the system in the solvent; thin dashed line, calculated data for the system adsorbed at a TiO$_2$ surface (for the parameters used, see Table 2).
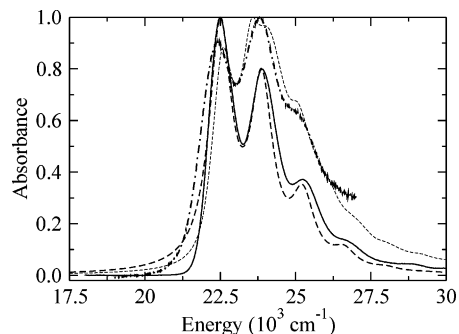
Figure 5. Rescaled linear absorption spectrum of the DTB−Pe−(CH$_2$)$_2$−COOH system: solid line, experimental data for the system in the solvent; dashed−dotted line, experimental data for the system adsorbed at a TiO$_2$ surface; thick dashed line, calculated data for the system in the solvent; thin dashed line, calculated data for the system adsorbed at a TiO$_2$ surface (for the parameters used, see Table 3).

The considered four examples introduced in Figure 1 differ in the bridge-anchor groups separating perylene from the surface with different distances. It is the advantage of these bridge-anchor groups that they realize different transfer couplings between the excited perylene state and the conduction band states of TiO$_2$. The strength of this coupling will be determined below by fitting the absorption spectra within the model introduced in the preceding sections. The measured data can be found in Figures 3−6. Note that we displayed in any case a rescaled absorbance, $\alpha(\omega)/\max \alpha(\omega)$ (or alternatively $\mathscr{D}(\omega)/\max \mathscr{D}(\omega)$).
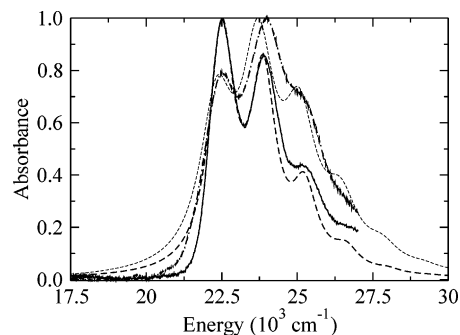
Figure 6. Rescaled linear absorption spectrum of the DTB−Pe−P(O)-(OH)$_2$ system: solid line, experimental data for the system in the solvent; dashed−dotted line, experimental data for the system adsorbed at a TiO$_2$ surface; thick dashed line, calculated data for the system in the solvent; thin dashed line, calculated data for the system adsorbed at a TiO$_2$ surface (for the parameters used, see Table 4).

A. Perylene Dyes in Solution. First, we discuss the results obtained for the absorption spectra of the dyes in a solvent (toluene/methanol, 1:1, see Figures 3−6). Computations of absorption spectra similar to the S$_0$−S$_1$ transition of dissolved perylene have been reported in a multitude of papers (see, e.g., refs 22 and 28). Provided that the curvature of the PES is parabolic and identical for the ground and the excited electronic states, the standard formula, eq A4, can be applied.

Absorption measurements performed at low temperature[20] and gas-phase fluorescence excitation spectra of perylene[29] show many active vibrational modes. The measured absorption spectra reported here, however, display the dominance of a single vibrational mode having a quantum energy, $\hbar\omega_{\mathrm{vib}}$, of about 0.17 eV (1370 cm^{-1}). This can be taken as a justification of the single-mode description which was used so far in refs 9−12 and which will be continued in this paper, too.

The neglect of any vibrational frequency change with the change of the electronic states allows for the introduction of a dimensionless vibrational coordinate, Q, which defines the PES as (remember the removal of the zero-point energy)

$$U_a(Q) = \hbar\omega_{\mathrm{vib}}(Q - Q_a)^2/4 - \hbar\omega_{\mathrm{vib}}/2 \qquad (10)$$

The equilibrium position of the PES is given by $Q_a = -2g_a$ (a = g, e, ion), where g_a denotes the dimensionless electron-vibrational coupling constant. The reorganization energy of a particular transition follows according to $\lambda_{ab} = \hbar\omega_{\mathrm{vib}}(g_a - g_b)^2 \equiv \hbar\omega_{\mathrm{vib}}(Q_a - Q_b)^2/4$. In this way, one obtains $\lambda_{\mathrm{eg}} = \hbar\omega_{\mathrm{vib}}(Q_e - Q_g)^2/4$, $\lambda_{\mathrm{ion\,e}} = \hbar\omega_{\mathrm{vib}}(Q_{\mathrm{ion}} - Q_e)^2/4$, and $\lambda_{\mathrm{ion\,g}} = \hbar\omega_{\mathrm{vib}}(Q_{\mathrm{ion}} - Q_g)^2/4$.

Figures 3−6 display a satisfactory reproduction of the vibrational progression indicating, in particular, that the single-coordinate description seems to be sufficient. Respective parameters are listed in Tables 1−4. The parameters of the different perylene bridge-anchor groups coincide very well except for the DTB−Pe−(CH)$_2$−COOH system, where the excited-state wave function extends into the bridge leading to a somewhat lower S$_1$-state energy. In particular, the data indicate a week influence of the bridge-anchor group on the overall perylene absorbance. Since a common level broadening, γ, has been used, the computed broadening of the 0−1 and 0−2 transitions is somewhat less than the measured one. Changing to a more involved description, for example, by including finite lifetimes of the vibrational levels via a coupling of the single mode to a heat bath of further vibrational modes, one automatically obtains an increase in the broadening for the 0−1 and 0−2 transitions. We will not introduce this possible improve-

Absorption Spectra Related to HET Reactions

J. Phys. Chem. B, Vol. 109, No. 19, 2005 **9593**

TABLE 1: Parameters of the DTB−Pe−COOH System in Solution (Pe−Solvent) and at the TiO$_2$ Surface (Pe−TiO$_2$) (A Respective Comparison between the Measured and Calculated Spectra Can Be Found in Figure 3)

	Pe−solvent	Pe−TiO$_2$
E_e (eV)	2.79	2.72
$\hbar\omega_{vib}$ (eV)	0.16	0.16
λ_{eg} (eV), ($Q_e - Q_g$)	0.116, (1.7)	0.187, (2.1)
$\hbar\gamma$ (eV)	0.062	0.062
E_{con} (eV)		1.79
ΔE_{con} (eV)		6.0
$\hbar\Gamma$ (eV)		0.069
$\lambda_{ion\,e}$ (eV), ($Q_{ion} - Q_e$)		0.014, (−0.6)

TABLE 2: Parameters of the DTB−Pe−(CH)$_2$−COOH System in Solution (Pe−Solvent) and at the TiO$_2$ Surface (Pe−TiO$_2$) (A Respective Comparison between the Measured and Calculated Spectra Can Be Found in Figure 4)

	Pe−solvent	Pe−TiO$_2$
E_e (eV)	2.65	2.65
$\hbar\omega_{vib}$ (eV)	0.17	0.17
λ_{eg} (eV), ($Q_e - Q_g$)	0.123, (1.7)	0.187, (2.1)
$\hbar\gamma$ (eV)	0.105	0.105
E_{con} (eV)		1.65
ΔE_{con} (eV)		6.0
$\hbar\Gamma$ (eV)		0.053
$\lambda_{ion\,e}$ (eV), ($Q_{ion} - Q_e$)		0.014, (−0.6)

TABLE 3: Parameters of the DTB−Pe−(CH$_2$)$_2$−COOH System in Solution (Pe−Solvent) and at the TiO$_2$ Surface (Pe−TiO$_2$) (A Respective Comparison between the Measured and Calculated Spectra Can Be Found in Figure 5)

	Pe−solvent	Pe−TiO$_2$
E_e (eV)	2.79	2.79
$\hbar\omega_{vib}$ (eV)	0.17	0.17
λ_{eg} (eV), ($Q_e - Q_g$)	0.123, (1.7)	0.187, (2.1)
$\hbar\gamma$ (eV)	0.058	0.058
E_{con} (eV)		1.79
ΔE_{con} (eV)		6.0
$\hbar\Gamma$ (eV)		0.021
$\lambda_{ion\,e}$ (eV), ($Q_{ion} - Q_e$)		0.014, (−0.6)

TABLE 4: Parameters of the DTB−Pe−P(O)(OH)$_2$ System in Solution (Pe−Solvent) and at the TiO$_2$ Surface (Pe−TiO$_2$) (A Respective Comparison between the Measured and Calculated Spectra Can Be Found in Figure 6)

	Pe−solvent	Pe−TiO$_2$
E_e (eV)	2.79	2.79
$\hbar\omega_{vib}$ (eV)	0.17	0.17
λ_{eg} (eV), ($Q_e - Q_g$)	0.132, (1.78)	0.225, (2.3)
$\hbar\gamma$ (eV)	0.063	0.043
E_{con} (eV)		1.79
ΔE_{con} (eV)		6.0
$\hbar\Gamma$ (eV)		0.037
$\lambda_{ion\,e}$ (eV), ($Q_{ion} - Q_e$)		0.014, (−0.6)

ment of our description here but state that the correct reproduction of the relative heights of the 0−0, 0−1, and 0−2 transitions in all considered cases represents a strong argument for the single-mode picture. Noting the recent normal-mode analysis for perylene presented in ref 30, we may identify our single vibration (with vibrational quantum energy in the 1370 cm^{-1} (0.17 eV) range) with a perylene in-plane C−C stretching vibration.

Finally, we will confront the parameters obtained here with those of ref 31 where electronic structure calculations on perylene have been reported. In particular, a reorganization energy, λ_{eg}, of 0.18 eV could be obtained which is a little bit larger than all that what has been deduced here in the single-mode description (the related displacement amounts to $Q_e -$

$Q_g = 2.06$). This discrepancy may result from the fact that gas-phase calculations have been carried out in ref 31.

B. Perylene Dyes Attached to the TiO$_2$ Surface. The absorption spectra related to perylene attached via different bridge-anchor groups to the surface of TiO$_2$ nanocrystals are also shown in Figures 3−6. For the DTB−Pe−COOH−TiO$_2$ and DTB−Pe−(CH)$_2$−COOH−TiO$_2$ systems, the vibrational progression found in the solvent is lost in the adsorbed state and an almost structureless absorption band appears instead (cf. Figures 3 and 4). In contrast, the DTB−Pe−(CH$_2$)$_2$−COOH− TiO$_2$ and DTB−Pe−P(O)(OH)$_2$−TiO$_2$ systems, Figures 5 and 6, respectively, retained the vibrational progression in the adsorbed states but with the 0−1 transition becoming stronger than the 0−0 transition. The trend observed in the absorption spectra, that is, the different degrees of broadening, for the surface attached case follows the intuitive expectation based on the molecular structure of the different bridge-anchor groups (see Figure 1).

To simulate the respective spectra, we have to make further assumptions concerning some additional parameters; that is, it becomes necessary to specify the energetic position and width of the TiO$_2$ conduction band as well as the DOS, eq 1. Moreover, the position of the PES for the cationic state of the dye (the reorganization energy, $\lambda_{ion\,e}$) and the frequency-dependent transfer coupling, $V_e(\omega)$, have to be fixed. In the following, we will discuss the calculated curves addressing the different experimental data.

As it has to be expected, the alternative computation of the absorbance (or the combined DOS) presented in ref 26 shows that the DOS, $\mathcal{N}(\omega)$, and $V_e(\omega)$ determine the spectra in a combined manner via the self-energy, eq 8. Since the injection position of the excited dye level is in a rather midband arrangement, it seems reasonable to use frequency-independent mean values $\bar{\mathcal{N}}$ and $\bar{V}_e$. Then, both can be combined to yield the frequency-independent expression for the line broadening (cf. eq 8)

$$\Gamma = \frac{\pi}{\hbar^2}\bar{\mathcal{N}}|\bar{V}_e|^2 \equiv -Im\Sigma \qquad (11)$$

The values of Γ for the different examples resulting from the fit are given in Tables 1−4 together with the other parameters (since $\bar{\mathcal{N}}$ and $\bar{V}_e$ independently enter our calculations, we fixed $\bar{\mathcal{N}}/\hbar$ at 2/eV and varied $\bar{V}_e$). The position of the excited state is on the order of 1 eV above the band edge,[14] and the bandwidth, ΔE_{con}, is set to 6 eV, as suggested by DFT computations.[23,31] The horizontal positioning of the PES minimum of the cationic state near that of the ground state (see Figure 2) follows the calculations of ref 31 where the relaxed nuclear configuration of the perylene cation has been found between the ground-state configuration and the excited-state configuration.

The calculated spectra (Figures 3−6) show an overall good agreement with the measured data. Let us first turn to the DTB− Pe−COOH−TiO$_2$ system (Figure 3), which displays the largest line broadening whereby nearly all the vibrational features disappear from the spectrum. The shift of the absorbance to the red wavelength range compared to the solvent case and the broadening of the absorption band can be reproduced by a decrease in the 0−0 transition energy in the adsorbed state and a line broadening, Γ, of 69 meV. Due to an increase in λ_{eg}, the maximum in the absorption curve shifts from the 0−0 to 0−1 transition (see the discussion below). The parameters of the calculated spectra are summarized in Table 1. The system DTB−Pe−(CH)$_2$−COOH−TiO$_2$ shows a similar behavior.

TABLE 5: Comparison of Charge Injection Times: Rate Equation Fit of the Measured Data (cf. ref 17) and Inverse of the HET Rate, eq B2

	$\tau_{\text{inj}}^{\text{(exp)}}$ (fs)	$1/k_{\text{HET}}$ (fs)
DTB−Pe−COOH−TiO$_2$	13	5
DTB−Pe−(CH)$_2$−COOH−TiO$_2$	10	6
DTB−Pe−(CH$_2$)$_2$−COOH−TiO$_2$	57	16
DTB−Pe−P(O)(OH)$_2$−TiO$_2$	28	9

This characteristic change of the relative heights in the vibrational progression upon adsorption becomes more obvious for the DTB−Pe−(CH)$_2$−COOH−TiO$_2$ and DTB−Pe−P(O)-(OH)$_2$−TiO$_2$ systems. As in the foregoing example, it is explained as a change of λ_{eg}, that is, as a change in the position of the excited-state PES when changing from the solvent to the surface attached case. We consider this assumption as the most plausible explanation, since increasing $Q_{\text{e}} - Q_{\text{g}}$ changes the relative heights of the 0−0 transition to the 0−1 transition. Obviously, the increase of $Q_{\text{e}} - Q_{\text{g}}$ results in an increase of the reorganization energy, λ_{eg}, as one may note from Tables 1−4.

In contrast to the distinct dependence of the spectra on λ_{eg}, they react less sensitive when changing the reorganization energy, $\lambda_{\text{ion e}}$, characterizing the charge injection. To fix $\lambda_{\text{ion e}}$, we may relate it to the computations of ref 31 or to the somewhat older measurement of photoelectron spectra.[27] Using the latter data, we arrive at the common value given in Tables 1−4. It corresponds to a $\lambda_{\text{ion g}}$ value of about 0.09 eV except for DTB−Pe−P(O)(OH)$_2$−TiO$_2$ where it reaches a value of 0.122 eV.

The value $\lambda_{\text{ion g}} = 0.05$ eV deduced from gas-phase computations on perylene without anchor groups[31] appears to be somewhat smaller. However, the deviation is not large and may be related to the somewhat different situation studied in ref 31. According to the given value of $\lambda_{\text{ion g}}$, one obtains in the single-mode description $Q_{\text{ion}} - Q_{\text{g}} = 1.09$, leading to $Q_{\text{ion}} - Q_{\text{e}} = -1.01$.

C. Absorption Line Broadening and Charge Injection Times. So far, exclusively frequency-domain spectra have been considered. Of course, it would be of interest to check the results as well as the validity of the model used by comparing them with independent measurements, for example, transient absorption data. Respective experiments have been carried out for the same experimental systems with a sufficiently high time resolution.[8,14,32] The measured injection times, τ_{inj}, range from 10 to nearly 60 fs and are summarized in Table 5.

To relate the measured data to those obtained from the simulation of stationary absorption spectra, one may choose the inverse of the HET rates, k_{HET}, eq B2. The respective values are also given in Table 5. The time constants obtained from the calculations reproduce the qualitative trend of the measured injection time constants.

V. Conclusions

The linear absorption spectra of perylene attached to nanostructured TiO$_2$ have been studied experimentally as well as theoretically. A theoretical fit of the measured data has been achieved in applying a time-dependent formulation of the absorbance. The description fully accounts for the electronic coupling to the conduction band continuum of TiO$_2$. Moreover, it uses a single reaction coordinate which corresponds to a perylene in-plane C−C stretching vibration with a quantum energy of 1370 cm^{-1}. The electronic coupling responsible for the heterogeneous electron transfer (HET) could be varied by inserting different bridge-anchor groups.

Our simulations reproduce the dye absorbance in a solvent and the trends in the line broadening of the vibrational progression due to the coupling to the conduction band continuum rather well. Respective HET rates deduced from these calculations follow the qualitative trend obtained from measurements on transient absorption. Quantitatively, however, the HET rates are systematically overestimated. This might be a consequence of the minimal single-mode model. The incorporation of additional modes into the model would improve the simulation of the experimental spectra but introduce significantly more parameters. Therefore, the procedure of fitting the absorption spectra by just one dominant vibrational mode appears justified, since it is sufficient for establishing the same systematic qualitative trend in the line widths of the absorption spectra and in the corresponding rate constants for electron transfer when different bridge-anchor groups are inserted between electron donor and electron acceptor.

However, multismode simulations of the stationary and transient absorbance based on electronic structure calculations are just under work.

Appendix A: Computation of the Absorption Coefficient

This appendix offers some details on the calculation of the frequency-dependent linear absorption. We start with eq 7 where the combined DOS has been introduced. Since the square of the transition-dipole matrix element appears explicitly in eq 7, the combined DOS takes the following form

$$\mathscr{D}_{\text{abs}}(\omega) = \frac{1}{\pi\hbar} Re \int_0^\infty dt\, e^{i\omega t} \times$$
$$\text{tr}_{\text{vib}}\{\langle\varphi_{\text{e}}|(\mathscr{U}_{\text{mol-sem}}(t)[\hat{r}_{\text{g}}|\varphi_{\text{e}}\rangle\langle\varphi_{\text{g}}|])|\varphi_{\text{g}}\rangle\} \quad \text{(A1)}$$

When deriving this expression, antiresonance contributions (resonances at negative frequencies) have been neglected. The equilibrium statistical operator, $\hat{W}_{\text{eq}}$, is set equal to $\hat{r}_{\text{g}}|\varphi_{\text{g}}\rangle\langle\varphi_{\text{g}}|$; that is, it describes vibrational equilibrium (with density operator $\hat{r}_{\text{g}}$) in the electronic ground state. If expanded with respect to the vibrational eigenstates, $\chi_{\text{g}N}$, of the vibrational Hamiltonian, H_{g}, the density operator of the vibrational equilibrium is given by $\hat{r}_{\text{g}} = \sum_N f(E_{\text{g}} + \hbar\omega_{\text{g}N})|\chi_{\text{g}N}\rangle\langle\chi_{\text{g}N}|$ (f denotes the respective thermal distribution, with $E_{\text{g}} + \hbar\omega_{\text{g}N}$ being the related energy, cf. eq 3). In eq A1, the trace with respect to the vibrational states is denoted by $\text{tr}_{\text{vib}}\{ \dots \}$, and time evolution follows from the action of the superoperator, $\mathscr{U}_{\text{mol-sem}}(t)$.

If any dissipative effect is neglected (for a more detailed discussion, see, for example, refs 25 and 33 and a forthcoming paper), $\mathscr{U}_{\text{mol-sem}}(t)$ reduces to the application of $\exp(-iH_{\text{mol-sem}}t/\hbar)$ from the left and the Hermitian conjugated version from the right. It yields

$$\mathscr{D}_{\text{abs}}(\omega) = \frac{1}{\pi\hbar} Re \int_0^\infty dt\, e^{i(\omega - \omega_{\text{eg}})t} \text{tr}_{\text{vib}}\{\hat{r}_{\text{g}} e^{iH_{\text{g}}t/\hbar} U_{\text{vib}}^{\text{(eff)}}(t)\} \quad \text{(A2)}$$

The transition frequency from the ground state to the excited electronic state is denoted by $\omega_{\text{eg}} = \omega_{\text{e}} - \omega_{\text{g}}$, and an effective vibrational time-evolution operator has been introduced which reads:

$$U_{\text{vib}}^{\text{(eff)}}(t) = e^{i\omega_{\text{e}}t}\langle\varphi_{\text{e}}|e^{-iH_{\text{mol-sem}}t/\hbar}|\varphi_{\text{e}}\rangle \quad \text{(A3)}$$

Absorption Spectra Related to HET Reactions

J. Phys. Chem. B, Vol. 109, No. 19, 2005 **9595**

Since an excited-electronic-state matrix element has been taken, the electronic ground state of the dye does not contribute.

Before proceeding further, let us shortly recall how the standard relation for $\mathscr{D}_{abs}$ is obtained if the coupling to the conduction band is neglected. In this case, $U_{vib}^{(eff)}(t)$ has to be replaced by $\exp(iH_et/\hbar)$. Assuming, additionally, a parabolic PES whose curvature is independent of the electronic state, one obtains for the combined DOS (cf., e.g., ref 25)

$$\mathscr{D}_{abs}(\omega) = \frac{1}{2\pi\hbar}\int dt\, e^{i(\omega-\omega_{eg})t - G(0) + G(t)} \quad (A4)$$

with the so-called line shape function

$$G(t) = \frac{1}{4}\sum_{\xi}(Q_e(\xi) - Q_g(\xi))^2 \times [(1 + n(\omega_\xi))e^{-i\omega_\xi t} +$$

$$n(\omega_\xi)e^{i\omega_\xi t}] \quad (A5)$$

Here, $Q_e(\xi)$ ($Q_g(\xi)$) defines the displacement of the excited-state (ground-state) PES versus the ξ'th (dimensionless) vibrational coordinate with frequency ω_ξ ($n(\omega_\xi)$ denotes the Bose distribution).

For the following computations, we will concentrate on a situation where only the vibrational ground state, χ_{g0}, of the electronic ground state is populated (presence of low temperatures and/or exclusively high-frequency vibrational modes or both). Then, eq A2 reduces to (remember that χ_{g0} belongs to $\omega_{g0} = 0$)

$$\mathscr{D}_{abs}(\omega) = \frac{1}{\pi\hbar}Re\int_0^\infty dt\, e^{i(\omega-\omega_{eg})t}\langle\chi_{g0}|U_{vib}^{(eff)}(t)|\chi_{g0}\rangle \quad (A6)$$

This formula together with eq A3 demonstrates that the state vector

$$|\Psi_0\rangle = |\chi_{g0}\rangle|\varphi_e\rangle \quad (A7)$$

has to be propagated under the action of the complete Hamiltonian, $H_{mol-sem}$, eq 2 (the absence of any ground-state excited-state coupling in $H_{mol-sem}$, however, eliminates any ground-state contribution). To solve the time-dependent Schrödinger equation, an expansion with respect to the diabatic electron-vibrational states, $|\chi_{aM}\rangle|\varphi_a\rangle$ (with a restricted to e and **k**), is introduced. The related expansion coefficients $C_{aM}(t)$ fulfill the initial condition

$$C_{aM}(0) = \delta_{a,e}\langle\chi_{eM}|\chi_{g0}\rangle \quad (A8)$$

According to this treatment, one obtains

$$\langle\chi_{g0}|U_{vib}^{(eff)}(t)|\chi_{g0}\rangle = \sum_M e^{i\omega_e t}\langle\chi_{g0}|\chi_{eM}\rangle C_{eM}(t) \quad (A9)$$

which leads to eq 9 for the combined DOS.

Appendix B: Rate of Heterogeneous Electron Transfer

To shortly establish the relation between the absorption line broadening and the finite lifetime of the vibrational levels of the excited electronic dye state, we present the rate of HET. One obtains

$$k_{HET} = \frac{2\pi}{\hbar}\sum_{M,N}P(\omega_{eM})|\langle\chi_{eM}|\chi_{ion\,N}\rangle|^2\int d\Omega\, \mathscr{N}(\Omega) \times$$

$$|V_e(\Omega)|^2\delta(E_e + \hbar\omega_{eM} - E_{con} - \hbar\omega_{ion\,N} - \hbar\Omega) \quad (B1)$$

where $P(\omega_{eM})$ denotes the population versus the vibrational levels of the first excited electronic state of the dye after photoexcitation (of course, this is not necessarily an equilibrium distribution). If one assumes a weak frequency dependence of the DOS and the coupling function, $V_e(\Omega)$, and replaces both by the appropriate averages, $\bar{\mathscr{N}}$ and $\bar{V}_e$, respectively, it is easy to show that the rate follows as (cf. also ref 34)

$$k_{HET} = \frac{2\pi}{\hbar^2}\bar{\mathscr{N}}|\bar{V}_e|^2 \equiv 2\Gamma \quad (B2)$$

As it has to be expected, the relation demonstrates that the transfer rate follows as 2 times the line broadening, eq 11.

References and Notes

(1) Adams, D. M.; et al. *J. Phys. Chem. B* **2003**, *107*, 6668.

(2) Miller, R. J. D.; McLendon, G.; Nozik, A.; Schmickler, W.; Willig, F. *Surface Electron Transfer Processes*; VCH Publishers: New York, 1995.

(3) O'Regan, B.; Grätzel, M. *Nature* **1991**, *353*, 737.

(4) Kallioinen, J.; Benkö, G.; Sundström, V.; Korppi-Tommola, J. E. I.; Yartsev, A. P. *J. Phys. Chem. B* **2002**, *106*, 4396.

(5) Hagfeldt, A.; Grätzel, M. *Chem. Rev.* **1995**, *95*, 49.

(6) Schwarzburg, K.; Ernstorfer, R.; Felber, S.; Willig, F. *Coord. Chem. Rev.* **2004**, *248*, 1259.

(7) Asbury, J. B.; Hao, E.; Wang, Y.; Ghosh, H. N.; Lian, T. *J. Phys. Chem. B* **2001**, *105*, 4545.

(8) Ernstorfer, R.; Gundlach, L.; Felber, S.; Storck, W.; Eichberger, R.; Willig, F. Manuscript to be published.

(9) Ramakrishna, S.; Willig, F.; May, V. *Phys. Rev. B* **2000**, *62*, R16330.

(10) Ramakrishna, S.; Willig, F.; May, V. *Chem. Phys. Lett* **2002**, *351*, 242.

(11) Ramakrishna, S.; Willig, F.; May, V.; Knorr, A. *J. Phys. Chem. B* **2003**, *107*, 607.

(12) Wang, L.; May, V. *J. Chem. Phys.* **2004**, *121*, 8039.

(13) Napper, A. M.; Read, I.; Kaplan, R.; Zimmt, M. B.; Waldeck, D. H. *J. Phys. Chem. A* **2002**, *106*, 5288.

(14) Ernstorfer, R.; Töben, L.; Gundlach, L.; Felber, S.; Galoppini, E.; Wei, Q.; Eichberger, R.; Storck, W.; Zimmermann, C.; Willig, F. *Proc. SPIE-Int. Soc. Opt. Eng.* **2003**, *5223*, 110.

(15) Burfeindt, B.; Hannappel, Th.; Storck, W.; Willig, F. *J. Phys. Chem.* **1996**, *100*, 16463.

(16) Zimmermann, C.; Willig, F.; Ramakrishna, S.; Burfeindt, B.; Pettinger, B.; Eichberger, R.; Storck, W. *J. Phys. Chem. B* **2001**, *105*, 9245.

(17) Gundlach, L.; Ernstorfer, R.; Felber, S.; Storck, W.; Eichberger, R.; Willig, F. Manuscript to be published.

(18) Ge, N.-H.; Wong, C. M.; Lingle Jr., R. L.; McNeill, J. D.; Gaffney, K. J.; Harris, C. B. *Science* **1998**, *279*, 202.

(19) Ramakrishna, S.; Willig, F.; Knorr, A. *Surf. Sci.* **2004**, *558*, 159.

(20) Halasinski, T. M.; Weisman, J. L.; Ruiterkamp, R.; Lee, T. J.; Salama, F.; Head-Gordon, M. *J. Phys. Chem. A* **2003**, *107*, 3660.

(21) Joblin, C.; Salama, F.; Allamandola, L. *J. Chem. Phys.* **1999**, *110*, 7287.

(22) Worth, G.; Meyer, H.-D.; Cederbaum, L. S. *J. Chem. Phys.* **1998**, *109*, 3518.

(23) Persson, P.; Bergström, R.; Lunell, S. *J. Phys. Chem. B* **2000**, *104*, 10348.

(24) Moser, J.; Punchihewa, S.; Infelta, P. P.; Grätzel, M. *Langmuir* **1991**, *7*, 3012.

(25) May, V.; Kühn, O. *Charge and Energy Transfer Dynamics in Molecular Systems*; Wiley-VCH: Berlin, 2004.

(26) Wang, L.; Willig, F.; May, V. *Chem. Phys.*, submitted for publication.

(27) Boschi, R.; Murrell, J. N.; Schmidt, W. *Faraday Discuss. Chem. Soc.* **1972**, *54*, 116.

(28) Egorov, S. A.; Rabani, E.; Berne, B. J. *J. Chem. Phys.* **1998**, *108*, 1407.

(29) Sulkes, M. *Chem. Phys.* **1987**, *114*, 289.

(30) Ong, K. K.; Jensen, J. O.; Hameka, H. F. *J. Mol. Struct.* **1999**, *459*, 131.

(31) Persson, P.; Lundqvist, M. J.; Borg A. Manuscript to be published.

(32) Ernstorfer, R.; Gundlach, L.; Felber, S.; Storck, W.; Eichberger, R.; Willig, F.; Lundqvist, M. J.; Persson, P. Manuscript to be published.

(33) Mancal, T.; May, V. *Chem. Phys.* **2001**, *268*, 201.

(34) Lanzafame, J. M.; Miller, R. J. D.; Muenter, A. A.; Parkinsons, B. A. *J. Phys. Chem.* **1992**, *96*, 2820.